PHYSICAL REVIEW FLUIDS **2**, 092603(R) (2017)

How vortices and shocks provide for a flux loop in two-dimensional compressible turbulence

Gregory Falkovich[1,2,*] and Alexei G. Kritsuk[3,†]
[1] *Weizmann Institute of Science, Rehovot 76100, Israel*
[2] *Institute for Information Transmission Problems, Moscow 127994, Russia*
[3] *University of California, San Diego, 9500 Gilman Drive, La Jolla, California 92093-0424, USA*
(Received 18 April 2017; published 28 September 2017)

Large-scale turbulence in fluid layers and other quasi-two-dimensional compressible systems consists of planar vortices and waves. Separately, wave turbulence usually produces a direct energy cascade, while solenoidal planar turbulence transports energy to large scales by an inverse cascade. Here, we consider turbulence at finite Mach numbers when the interaction between acoustic waves and vortices is substantial. We employ solenoidal pumping at intermediate scales and show how both direct and inverse energy cascades are formed starting from the pumping scale. We show that there is an inverse cascade of kinetic energy up to a scale ℓ, where a typical velocity reaches the speed of sound; this creates shock waves, which provide for a compensating direct cascade. When the system size is less than ℓ, the steady state contains a system-size pair of long-living condensate vortices connected by a system of shocks. Thus turbulence in fluid layers processes energy via a loop: Most energy first goes to large scales via vortices and is then transported by waves to small-scale dissipation.

DOI: 10.1103/PhysRevFluids.2.092603

Inverse cascade is a counterintuitive process of self-organization of turbulence. Predicted almost simultaneously for two-dimensional (2D) incompressible flows [1] and sea wave turbulence [2] and established in many cases of turbulence in plasma, optics, etc. [3–8], it is predicated on the existence of two quadratic conserved quantities having different wave-number dependencies. Excitation at some intermediate wave number then leads to two cascades: a direct one to small scales and an inverse one to large scales. There is always a strong dissipation at small scales which acts as a sink for the direct cascade. On the contrary, large-scale motions are usually less dissipative, so that an inverse cascade can proceed unimpeded, either producing larger and larger scales or reaching the box size and creating a coherent mode of growing amplitude. That process is now actively studied in 2D incompressible turbulence [3,4,9–13], including in a curved space, where vortex rings rather than vortices are created [14]. The energy of an incompressible flow in an unbounded domain grows unlimited when the friction factors go to zero at a finite energy input rate. The same happens to the action of wave turbulence [15], if long waves of large amplitude are stable. For example, optical turbulence in media with defocusing nonlinearity produces a growing condensate [7,8,16]. On the contrary, in the focusing case, condensate instability results in wave collapses which provide for a loop of inverse cascade to the small-scale dissipation so that there is a steady state with only small-scale dissipation [8].

Here, we consider compressible two-dimensional turbulence which is of significant importance for numerous geophysical, astrophysical, and industrial applications. We show that it realizes a third possibility of a steady state with only small-scale dissipation: On the one hand, an inverse cascade is able to produce long-living stable vortices, and on the other hand, the system reaches a steady state as the vortices produce waves that break and dissipate the energy. Two-dimensional

*gregory.falkovich@weizmann.ac.il
†akritsuk@ucsd.edu

compressible hydrodynamics describes motions in fluid layers on scales exceeding the fluid depth when vortices are planar while waves are acoustic, the thickness playing the role of density. We consider an ideal-gas equation of state with the ratio of specific heats $\gamma = c_p/c_v \to 1$ (that is near isothermal) which is relevant to astrophysical systems (where radiation provides for temperature equilibration [17–24]) and for soap film flows with a large Reynolds number, a nonvanishing Mach number, and negligible solubility [25,26].

Our results may also relate to the shallow water model, which is basically described by the same set of equations, but with $\gamma = 2$. In this context, some of the potential applications include dissipation in geostrophic turbulence and its impact on the stability of mesoscale oceanic eddies [27]. A weak direct energy cascade was predicted in Ref. [28], using statistical mechanical arguments, which seemed in contradiction to the numerical results of Ref. [29]. A flux loop of a similar nature to the one discussed here perhaps might solve that paradox.

A flux loop was also observed in a relatively simpler case of weakly stratified 2D turbulence [30], where there is only one conserved quantity, so that an inverse cascade can exist only in a restricted interval of scales until the kinetic energy converts into the potential energy which cascades to small scales. Our case is more complicated and rich: first, because the energy, $E = K + W = \int[\rho u^2/2 + c^2\rho\ln(\rho/\rho_0)]d\boldsymbol{x}$, written here for an isothermal case (ρ is the density, ρ_0 the mean density, $\boldsymbol{u}$ the velocity, and c the sound speed), is both potential and kinetic, and also because the kinetic energy has two components, solenoidal and potential (dilatational). Second, smooth flows in ideal 2D compressible hydrodynamics conserve not only the energy integral but also the potential vorticity $\boldsymbol{\omega}/\rho$ of any streamline, where $\boldsymbol{\omega} = \nabla \times \boldsymbol{u}$. We characterize compressibility by the rms Mach number $M = \sqrt{\langle u^2\rangle}/c$. When compressibility is small, two cascades exist, much as in the incompressible case [31]. Indeed, the two relevant conserved quantities are close to quadratic: (i) The density times the squared potential vorticity, $H = \int \omega^2/\rho\, d\boldsymbol{x}$, goes into the direct cascade, and (ii) the (mostly kinetic) energy goes into the inverse cascade. As the vortices get larger and faster in the inverse cascade, they start to create density perturbations, thus increasing the potential energy along with the kinetic energy. Even when external pumping is weak, as the inverse cascade proceeds to larger scales, typical velocities increase and eventually become comparable to the speed of sound, while density perturbations become substantial. That allows for an effective interaction of vortices and waves and energy transfer from the former to the latter. Waves can then transfer energy back from large to small scales due to wave breaking and shock creation. We show that kinetic energy has an upscale flux above the force scale λ_f. Since we observe a steady state, then the return downscale flux must be of potential energy. What is remarkable is that the fluxes are independent of wave number k at $k < k_f \equiv 2\pi/\lambda_f$, thus representing cascades.

The description of numerical simulations [implicit large-eddy simulations (ILES) [32–35]] can be found in Ref. [17]. Before analyzing the steady state, let us describe the energy growth, saturation, and fluctuations. At small t, while $M < 0.2$, the kinetic part strongly dominates the energy balance. On average, the contribution of potential energy reaches $W \approx 0.1E$ at $M = 0.5$–0.7, as the total energy growth saturates. Remarkably, this 10% saturation level does not depend on the pumping rate ε_f. Simulations show that $K(t)$ and $W(t)$ are strongly coupled and oscillate with opposite phases. The oscillation amplitude grows with M and eventually saturates, reaching $W \approx 0.15E$ during dissipation bursts and decreasing to $0.07E$ during periods of more quiet evolution. The main characteristic frequency of such oscillations is determined by the sound speed c, rotation velocity profile of large-scale vortices $U(r)$, and mean intervortical separation $L/\sqrt{2}$ (L is the domain size). These large-scale acoustic oscillations represent a compressible component of the total condensate energy.

Figure 1 presents the evolution of energy and Mach number for the cases of weak (A, B, C), intermediate (D), and strong (E) pumping ε_f. In all cases, the energy evolution starts with a linear growth $E(t) = \varepsilon_f t$, which soon saturates due to a strong peak of small-scale compressible dissipation. After that, the inverse cascade is launched and linear growth resumes with a lower rate $\dot{E} = \varepsilon_g \sim 0.9\varepsilon_f$. As soon as the rms Mach number exceeds 0.3, shock dissipation starts to play a role and further slows down the energy growth to $\sim 0.4\varepsilon_f$. Somewhat later, a domain-size vortex dipole appears and then grows more coherent, as more energy is pumped in. The periods of slow

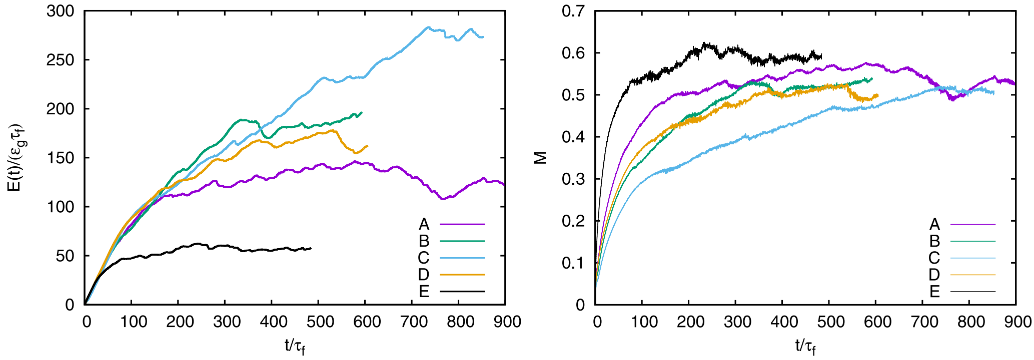

FIG. 1. Time evolution of the total energy (left) and the rms Mach number (right) for cases A–E. The time is normalized with the forcing time $\tau_f = \rho_0^{1/3}\lambda_f^{2/3}\varepsilon_f^{-1/3}$. Cases A–C form a sequence with increasing grid resolution, where each step adds a factor of 2 to the extent of both cascades in this dual-cascade setup.

growth are interrupted by episodic bursts of shock dissipation. For instance, the emergence of a single strong shock (pressure jump > 2), connecting the centers of large-scale vortices, can cause a sharp drop in $E(t)$ by several percent. As the bursts become more frequent at higher energy levels ($M > 0.5$), the overall growth slows down to below 10% and eventually saturates, but one can still see short patches of uninterrupted growth with the same characteristic rate of $0.4\varepsilon_f$ between the bursts. Bursts of dissipation are observed to be of a different nature. Some are correlated with the intermittent appearance of shocks across the large-scale vortex dipole that become particularly dramatic when the two vortices approach closely. Some other cases correspond to vortices being destroyed completely and then reappearing after a while. Deep energy minima are accompanied by intense oscillations of relative strength of the vortices in the pair as best seen in the density movie [17]; apparently, the large-scale acoustic mode causes strong dissipation [17,36–44]. During the time intervals when vortices stop oscillating and are comparable in magnitude, the energy continues approximately linear growth.

The evolution is different in run E, where condensate vortices do not appear, and the Mach number $M \simeq 0.6$ is reached at scales below the box size, leading to many midsize vortices being present at the saturated stage, which fluctuates much less as a result. Note that the energy in the left panel is normalized by pumping. As is clear from the right panel of Fig. 1, in all runs the typical velocities and total energy reach approximately the same values. Incidentally, it was reported that even a stable condensate does not appear in optical turbulence when the pumping is too strong [7]; whether there is a general phenomenon of inverse cascade disruption due to high effective nonlinearity (for instance, because integrals of motion cease to be quadratic) is poorly understood.

It is important that the decay or growth of total energy is determined by the shock (rather than total) dissipation; apparently, solenoidal dissipation, however large and finite the kinematic viscosity ν, is irrelevant to the inverse cascade.

Let us now analyze kinetic energy fluxes for states with different Mach numbers that appear at different pumping rates and in different boxes (Fig. 2 and Ref. [17]). Consider that we use solenoidal pumping so that at a low Mach number we have practically incompressible turbulence with most of the energy going to the left of the forcing scale, i.e., into the inverse cascade. We see that with increasing Mach number, the larger and larger fraction of kinetic energy goes to the right of the forcing scale, i.e., into the direct cascade. Still, the inverse cascade is well pronounced in all cases. At Mach numbers of order unity, approximately equal fluxes go to large and small scales (a turbulence version of energy equipartition). Figure 3 shows the spectra of kinetic and potential energy and also separately the spectrum of the kinetic energy of potential (dilatational) part of the velocity field. We see that $W(k) \ll K(k)$ for most k, yet their fluxes must be comparable to provide for a steady state. This is an extra reminder how different (and complementary) information is brought by analyzing

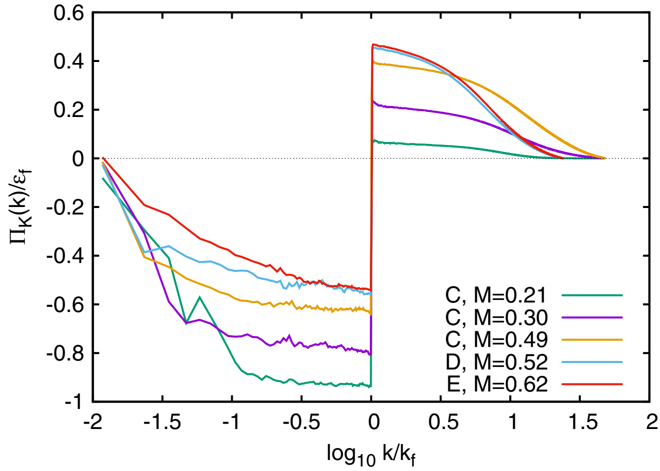

FIG. 2. Kinetic energy fluxes for the case C at $M = 0.21$ and 0.30 (nonstationary, no condensate) and $M = 0.49$ (quasistationary with condensate); D at $M = 0.52$ (quasistationary with condensate); E at $M = 0.62$ (quasistationary, no condensate). Fluxes saturate at $\Pi_K \approx \pm 0.5\varepsilon_f$ as the Mach number approaches 0.6, apparently due to a direct acoustic energy flux that matches the energy injection rate at $M \geqslant 0.6$, halts the total energy growth, and forms a closed energy flux loop at $k > k_f$.

together the spectra and fluxes. We also see that the dilatational part of the kinetic energy is small all the way to $k \simeq 10k_f$, so that the kinetic energy of vortices dominates. Only at $k > 10k_f$ do the waves dominate and kinetic and potential energies and fluxes are getting equal, as it must be in weak turbulence [15].

Turbulence at scales smaller than the force scale can be naturally assumed to carry the direct energy flux provided by acoustic waves. This is supported by the spectra, which show that at $k \gtrsim k_f$ the potential energy is equal to the dilatational energy and both decay as k^{-2}, as expected for acoustic turbulence [15]. Of course, there is more to turbulence at $k > k_f$ than the energy cascade. It must also carry the cascade of H which it does by the solenoidal part of the velocity field whose vorticity spectrum behaves as $k^{-1}\ln^{-1/3}(k/k_f)$, in exact correspondence to the theory of the enstrophy cascade in incompressible turbulence [1,45]. An effective Mach number decreases towards small scales so that vortices and waves are getting decoupled. Since the vortical contribution decays faster, waves

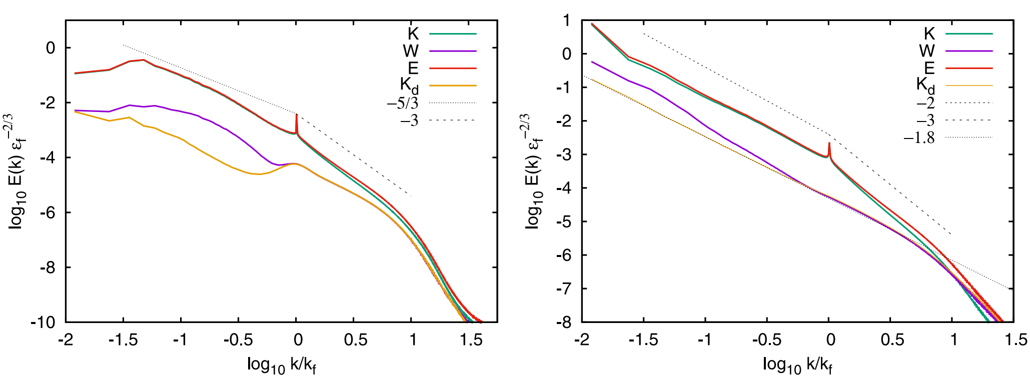

FIG. 3. Energy spectra for case C at $M = 0.2$ (left) and 0.5 (right); see Refs. [17,46–49] for definitions in the compressible case.

dominate kinetic energy for the small-scale part of the spectra. For most wave numbers, however, the energy of the vortices is dominant.

Let us now look at turbulence at scales above the force scale. It is likely that the acoustic direct energy cascade originates at scales far exceeding the force scale and goes through it. This is evidenced by the spectra of potential and dilatational kinetic energy which behave continuously through k_f. On the contrary, the solenoidal part of the kinetic energy has a narrow peak right at $k = k_f$ and the kinetic energy flux Π_K jumps from Π_W at $k > k_f$ to $-\Pi_W$ at $k < k_f$, so that the total energy flux towards large scales is zero.

It deserves attention that the low-Mach energy spectra at $k < k_f$ in the left panel are usual $k^{-5/3}$, while the spectra are close to k^{-2} in the right panel of Fig. 3. However tempting it is to ascribe this to shock waves, this is not the case since the spectra are overwhelmingly dominated by the kinetic energy of solenoidal motions, i.e., vortices. That means that even though density variations are substantial only at large scales (where the Mach number is not small), they modify vortices and affect spectra at all scales down to the pumping scale. Our compressible spectrum climbs towards small k faster than the $-5/3$ spectrum of an inverse cascade with a large-scale sink (yet slower than the k^{-3} spectrum of the large-scale coherent vortex [4]). To interpret this, recall that the mechanism of inverse cascade is the deformation of small vortices inside a large one and the back reaction which reinforces the large vortex [50]. In a compressible case, the fact that the spectrum is steeper may mean that for a cascade to proceed, the ratio between energies of the larger vortex and smaller vortices inside it must be larger than in an incompressible case.

That potential energy exceeds dilatational energy at large scales is extra evidence that density perturbations are related not only to waves but also to vortices. Note that a similar detailed energy equipartition across scales is seen in three dimensions (3D) at $M \approx 0.6$ [51,52].

When the inverse cascade reaches the system size and creates coherent vortices, their main dissipation is at the shocks, which go out of the vortex centers, connect them, and create spiral structures around them. Apart from a purely fluid-mechanical interest, the spontaneous formation of strong vortices with shocks in compressible quasi-2D flows may influence different astrophysical phenomena, for instance, in the contexts of disk accretion [54], galactic disks [55], or planetesimal formation in protoplanetary disks [56]. Here, we focus on analyzing the vortex structure and the energy-momentum fluxes that support the coherent vortex. To appreciate better the peculiarities of the compressible case, let us briefly remind that in the incompressible case the inverse cascade produces a pair of vortices with a narrow viscous core, outside of which the mean azimuthal velocity is independent of the radius, $U = \sqrt{3\varepsilon_f/\alpha\rho}$, where α is the rate of uniform (bottom) friction [10]. Each vortex is sustained by the inward radial momentum fluxes. The (radial) flux of the radial momentum is provided mostly by the mean pressure, $\rho U^2 \approx r dP/dr$. The flux of the azimuthal momentum is provided by fluctuations, $\tau = \rho\langle uv\rangle = r\sqrt{\rho\varepsilon_f\alpha/3}$, where u,v are respectively azimuthal and radial fluctuating velocities in a reference frame comoving with the vortex center. For the flat profile, the turbulence-vortex energy exchange rate per unit area, $F_1 = r^{-1}\partial_r rU\tau = 2\varepsilon_f$, is also independent of the radius and equal to twice the input rate; the turbulence flux divergence $F_2 = r^{-1}\partial_r r\langle v(\rho u^2 + \rho v^2 + 2p)\rangle/2$ is negligible [10]. All the energy input from the external pumping and turbulence inverse cascade is dissipated inside the vortex by linear friction, $\alpha\rho U^2 = 3\varepsilon_f$.

For the compressible case which we consider, there is no bottom friction and, consequently, no momentum loss from the system. Averaging the continuity equation for the density of angular momentum and taking into account that the mass flux $\langle\rho v\rangle$ must be zero, we get inside the vortex the condition for total zero momentum flux,

$$\langle\rho vu\rangle = \nu\Sigma r\frac{\partial}{\partial r}\frac{U}{r} + \left\langle\frac{\nu\rho}{r}\frac{\partial v}{\partial\phi}\right\rangle + r\left\langle\nu\rho\frac{\partial}{\partial r}\frac{u}{r}\right\rangle. \quad (1)$$

Since the mean density and velocity profiles $\Sigma(r)$ and $U(r)$ are smooth, then the first term on the right-hand side (rhs) goes to zero with ν. It is thus clear that inertial momentum flux $\tau = \langle\rho uv\rangle$ could be nonzero only if there is a finite inviscid limit of the last two terms on the rhs, which are due to turbulence. That requires tangential discontinuities, apparently provided by the spiral shocks

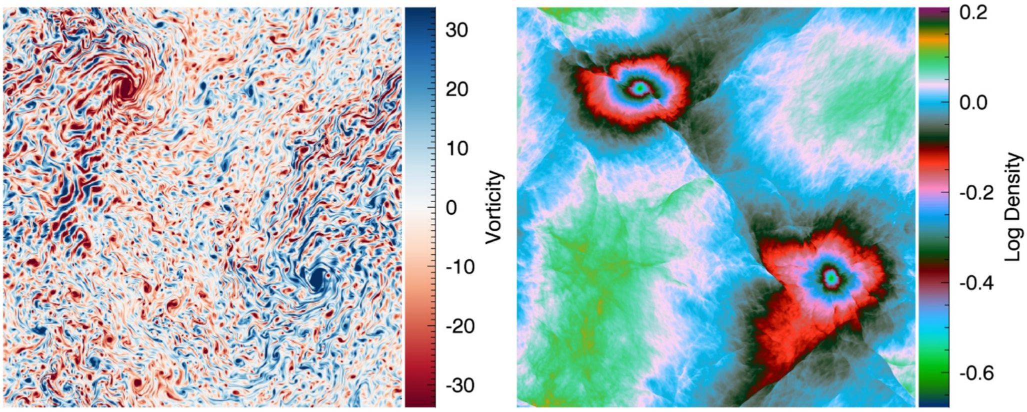

FIG. 4. Vorticity and density fields in model B at $t = 412$. (See Ref. [17] for animations and visuals generated using the line integral convolution technique [53].)

coming out of the vortices and long shocks connecting vortex centers which we observe. Movies [17] also show density profiles strongly corrugated along ϕ and fast changing along r, which is conducive to having $\tau \neq 0$. Most likely, the mechanism of nonzero viscous momentum transfer at the inviscid limit is the angle change of a streamline after passing through shock. For that one indeed needs spiral-like shocks, which deflect streamlines out. If the shock deflects against the vortex flow, then the rhs of (1) is negative, as can be expected (inertia brings momentum in, and viscous friction takes it out). Only with nonzero inertial momentum flux into a vortex can the inertial energy flux into vortex $\tau r \partial_r (U/r)$ be nonzero as well. We expect the energy input rate ε_f to exceed the viscous energy dissipation outside the vortices, so that the energy must flow into the vortices to be dissipated there.

A typical snapshot of the vorticity and density fields in the energy-saturated state with a condensate is shown in Fig. 4. To compute the averages, we save 20 flow snapshots per crossing time; with these we can create reasonably smooth animations [17] and robustly decompose the mean flow from the turbulence, using an algorithm similar to that of Ref. [10] with some modifications to account for compressibility [17]. One learns from case C that the condensate vortex has a circular core with a vorticity comparable to several other vortices present at any given time; what distinguishes the condensate vortex is a spiral around the core so that the density is perturbed in the whole region, core and spiral, which provides for strong dissipation. Secondary vortices, on the contrary, do not perturb density in any substantial way. Most of the time, the vortex as a whole moves generally with a speed much less than the flow velocity in the vortex itself, so one can neglect distortions caused by the center motion.

As in Ref. [10], the mean vorticity profile within a coherent vortex is close to isotropic, but the 2D density distribution shows shallow diagonal minima, resembling the density depressions along the lines connecting the vortices in individual snapshots (Fig. 4). The mean flow is characterized by the azimuthally averaged density and velocity profiles $\Sigma(r)$ and $U(r)$, shown in the left panel of Fig. 5 for case C. We see that the density decreases monotonically towards the center, while the velocity grows and then decays. As the vortex grows, the outer velocity profile flattens. What matters, however, is the comparison of the centrifugal force $\Sigma U^2/r$ and the radial pressure gradient $dP/dr = c^2 d\Sigma/dr$. It is more convenient to compare U^2 with $c^2 d \ln \Sigma / d \ln r \equiv c^2 \Sigma'$, which is done in the inset in Fig. 5. Remarkably, the radial balance of the momentum fluxes holds with an accuracy of a few percent already on the mean profiles, despite the quite complicated structure of the vortex, as seen in Figs. 4 and 5. In other words, the mean pressure and velocity satisfy the steady Euler equation, that is, the contribution of fluctuations into the radial momentum flux is negligible, even though the fluctuations are quite strong (and $U_{\max} \approx 0.7c$).

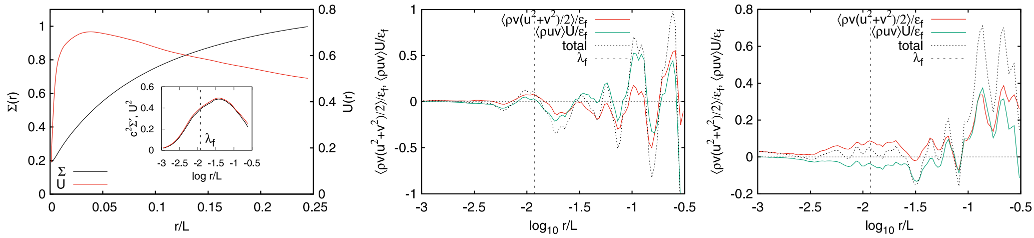

FIG. 5. Profiles of the mean density $\Sigma(r)$ and velocity $U(r)$ for the condensate in model C at $M \approx 0.5$, $t \in [380,400]$ (left panel). The inset illustrates the radial force balance for the mean flow. Time-averaged turbulent fluxes for case C at $t \in [283,300]$ (center) and $t \in [380,400]$ (right panel). The sum of two fluxes is shown by the dashed line; vertical lines indicate the forcing scale λ_f.

Fluctuations, however, play a crucial role in feeding energy and azimuthal momentum to the vortex, as shown in Fig. 5. We find that the fluxes here are quite different from the incompressible case: F_1, F_2 are comparable but they change sign along the radius (see Fig. 5 and Ref. [17]). Apparently, those oscillations are the signature of a spiral structure of shocks, so that the energy fluxes converge to shocks at spiral arms rather than to the vortex center.

Note that fluxes fluctuate strongly, so that a short-time average can often give an opposite sign of the energy fluxes, as seen from comparing the two right panels in Fig. 5. A positive (outward) angular momentum flux, as that observed here at some radii at the vortex periphery, was previously observed in the case of a rotating disk and ascribed to compressibility [54].

This research was supported in part by the National Science Foundation through Grant No. AST-1412271 as well as through XSEDE allocations on *Trestles*, *Gordon*, *Comet* supercomputers at SDSC as well as *Stampede* at TACC (projects MCA07S014 and SDSC-DDP189). The work of G.F. was supported by the RScF Grant No. 14-22-00259 and by the ISF Grant No. 712174. The authors gratefully acknowledge support from the Simons Center for Geometry and Physics, Stony Brook University, at which some of the research for this paper was performed. A.K. appreciates the warm hospitality of Weizmann Institute of Science during his visit in late 2016.

[1] R. H. Kraichnan, Inertial ranges in two-dimensional turbulence, Phys. Fluids **10**, 1417 (1967).
[2] V. E. Zakharov, Ph.D. thesis, Budker Institute for Nuclear Physics, Novosibirsk, 1967.
[3] P. Tabeling, Two-dimensional turbulence: A physicist approach, Phys. Rep. **362**, 1 (2002).
[4] H. Xia, M. Shats, and G. Falkovich, Spectrally condensed turbulence in thin layers, Phys. Fluids **21**, 125101 (2009).
[5] E. G. Turitsyna, G. Falkovich, V. K. Mezentsev, and S. K. Turitsyn, Optical turbulence and spectral condensate in long-fiber lasers, Phys. Rev. A **80**, 031804 (2009).
[6] G. Falkovich, Inverse Cascade and Wave Condensate in Mesoscale Atmospheric Turbulence, Phys. Rev. Lett. **69**, 3173 (1992).
[7] A. Dyachenko and G. Falkovich, Condensate turbulence in two dimensions, Phys. Rev. E **54**, 5095 (1996).
[8] A. Dyachenko, A. C. Newell, A. Pushkarev, and V. E. Zakharov, Optical turbulence: Weak turbulence, condensates and collapsing filaments in the nonlinear Schrodinger equation, Physica D **57**, 96 (1992).
[9] C. Chan, D. Mitra, and A. Brandenburg, Dynamics of saturated energy condensation in two-dimensional turbulence, Phys. Rev. E **85**, 036315 (2012).
[10] J. Laurie, G. Boffetta, G. Falkovich, I. Kolokolov, and V. Lebedev, Universal Profile of the Vortex Condensate in Two-Dimensional Turbulence, Phys. Rev. Lett. **113**, 254503 (2014).

[11] G. Falkovich, Interaction between mean flow and turbulence in two dimensions, Proc. R. Soc. A **472**, 20160287 (2016).
[12] I. V. Kolokolov and V. V. Lebedev, Structure of coherent vortices generated by the inverse cascade of two-dimensional turbulence in a finite box, Phys. Rev. E **93**, 033104 (2016).
[13] A. Frishman, J. Laurie, and G. Falkovich, Jets or vortices? What flows are generated by an inverse turbulent cascade?, Phys. Rev. Fluids **2**, 032602(R) (2017).
[14] G. Falkovich and K. Gawedzki, Turbulence on hyperbolic plane: The fate of inverse cascade, J. Stat. Phys. **156**, 10 (2014).
[15] V. E. Zakharov, V. S. L'vov, and G. Falkovich, *Kolmogorov Spectra of Turbulence* (Springer, Berlin, 1991).
[16] N. Vladimirova, S. Derevyanko, and G. Falkovich, Phase transitions in wave turbulence, Phys. Rev. E **85**, 010101 (2012).
[17] See Supplemental Material at http://link.aps.org/supplemental/10.1103/PhysRevFluids.2.092603 for a brief description of numerical experiments, technical details of the spectral energy density and flux calculation (Figs. 2 and 3), animations and complementary renderings for Fig. 4, and the procedure for vortex tracking and profiling relevant to Fig. 5.
[18] M. G. Wolfire, C. F. McKee, D. Hollenbach, and A. G. G. M. Tielens, Neutral atomic phases of the interstellar medium in the Galaxy, Astrophys. J. **587**, 278 (2003).
[19] G. B. Field, Thermal instability, Astrophys. J. **142**, 531 (1965).
[20] A. G. Kritsuk, Fine structure of emission filaments in the Cygnus Loop, Astrofizika **25**, 45 (1986).
[21] K. V. Krasnobaev and R. R. Tagirova, Isentropic thermal instability in atomic surface layers of photodissociation regions, Mon. Not. R. Astron. Soc. **469**, 1403 (2017).
[22] A. G. Kritsuk, S. D. Ustyugov, and M. L. Norman, The structure and statistics of interstellar turbulence, New J. Phys. **19**, 065003 (2017).
[23] C. F. McKee and E. C. Ostriker, Theory of star formation, Annu. Rev. Astron. Astrophys. **45**, 565 (2007).
[24] M. A. Martos and D. P. Cox, Magnetohydrodynamic modeling of a Galactic spiral arm as a combination shock and hydraulic jump, Astrophys. J. **509**, 703 (1998).
[25] J.-M. Chomaz, The dynamics of a viscous soap film with soluble surfactant, J. Fluid Mech. **442**, 387 (2001).
[26] P. Fast, A viscous compressible model of soap film flow and its equivalence with the Navier-Stokes equations, arXiv:physics/0511175.
[27] J. C. McWilliams, Submesoscale currents in the ocean, Proc. R. Soc. London, Ser. A **472**, 20160117 (2016).
[28] T. Warn, Statistical mechanical equilibria of the shallow water equations, Tellus A **38**, 1 (1986).
[29] M. Farge and R. Sadourny, Wave-vortex dynamics in rotating shallow water, J. Fluid Mech. **206**, 433 (1989).
[30] G. Boffetta, F. D. Lillo, A. Mazzino, and S. Musacchio, A flux loop mechanism in two-dimensional stratified turbulence, Europhys. Lett. **95**, 34001 (2011).
[31] J. P. Dahlburg, R. B. Dahlburg, J. H. Gardner, and J. M. Picone, Inverse cascades in two-dimensional compressible turbulence. I. Incompressible forcing at low Mach number, Phys. Fluids A **2**, 1481 (1990).
[32] I. V. Sytine, D. H. Porter, P. R. Woodward, S. W. Hodson, and K.-H. Winkler, Convergence tests for the piecewise parabolic method and Navier-Stokes solutions for homogeneous compressible turbulence, J. Comput. Phys. **158**, 225 (2000).
[33] F. F. Grinstein, L. G. Margolin, and W. Rider, *Implicit Large Eddy Simulation: Computing Turbulent Fluid Dynamics* (Cambridge University Press, Cambridge, UK, 2007).
[34] P. Colella and P. R. Woodward, The piecewise parabolic method (PPM) for gas-dynamical simulations, J. Comput. Phys. **54**, 174 (1984).
[35] G. Bryan *et al.*, ENZO: An adaptive mesh refinement code for astrophysics, Astrophys. J. Suppl. **211**, 19 (2014).
[36] H. Xu, A. Pumir, G. Falkovich, E. Bodenschatz, M. Shats, H. Xia, N. Francois, and G. Boffetta, Flight-crash events in turbulence, Proc. Natl. Acad. Sci. USA **111**, 7558 (2014).
[37] T. Grafke, A. Frishman, and G. Falkovich, Time-irreversibility of the statistics of a single particle in a compressible turbulence, Phys. Rev. E **91**, 043022 (2015).

[38] E. G. Broadbent and D. W. Moore, Acoustic destabilization of vortices, Philos. Trans. R. Soc. A **290**, 353 (1979).
[39] V. F. Kop'ev and E. A. Leont'ev, On acoustic instability of an axial vortex, Akust. Zh. **29**, 192 (1983).
[40] M. V. Melander, N. J. Zabusky, and J. C. McWilliams, Symmetric vortex merger in two dimensions—Causes and conditions, J. Fluid Mech. **195**, 303 (1988).
[41] S. Zhang, H. Li, X. Liu, H. Zhang, and C.-W. Shu, Classification and sound generation of two-dimensional interaction of two Taylor vortices, Phys. Fluids **25**, 056103 (2013).
[42] V. I. Klyatskin, Sound radiation by a system of vortices, Izv. Akad. Nauk SSSR, Mekh. Zhidk. Gaza **1**, 87 (1966).
[43] B. E. Mitchell, S. K. Lele, and P. Moin, Direct computation of the sound from a compressible co-rotating vortex pair, J. Fluid Mech. **285**, 181 (1995).
[44] K. A. Naugol'nykh, Nonlinear sound waves upon collapse of a vortex dipole, Acoust. Phys. **60**, 424 (2014).
[45] G. Falkovich and V. Lebedev, Universal direct cascade in two-dimensional turbulence, Phys. Rev. E **50**, 3883 (1994).
[46] S. Kida and S. A. Orszag, Energy and spectral dynamics in forced compressible turbulence, J. Sci. Comput. **5**, 85 (1990).
[47] P. Sagaut and C. Cambon, *Homogeneous Turbulence Dynamics* (Cambridge University Press, Cambridge, UK, 2008).
[48] S. Galtier and S. Banerjee, Exact Relation for Correlation Functions in Compressible Isothermal Turbulence, Phys. Rev. Lett. **107**, 134501 (2011).
[49] J. Wang, Y. Shi, L.-P. Wang, Z. Xiao, X. T. He, and S. Chen, Scaling and Statistics in Three-Dimensional Compressible Turbulence, Phys. Rev. Lett. **108**, 214505 (2012).
[50] S. Chen, R. E. Ecke, G. L. Eyink, M. Rivera, M. Wan, and Z. Xiao, Physical Mechanism of the Two-Dimensional Inverse Energy Cascade, Phys. Rev. Lett. **96**, 084502 (2006).
[51] S. Sarkar, G. Erlebacher, M. Y. Hussaini, and H. O. Kreiss, The analysis and modeling of dilatational terms in compressible turbulence, J. Fluid Mech. **227**, 473 (1991).
[52] S. Jagannathan and D. A. Donzis, Reynolds and Mach number scaling in solenoidally-forced compressible turbulence using high-resolution direct numerical simulations, J. Fluid Mech. **789**, 669 (2016).
[53] B. Cabral and L. C. Leedom, Imaging vector fields using line integral convolution, in *Proceedings of the 20th Annual Conference on Computer Graphics and Interactive Techniques* (ACM, New York, 1993), pp. 263–270.
[54] B. M. Johnson and C. F. Gammie, Vortices in thin, compressible, unmagnetized disks, Astrophys. J. **635**, 149 (2005).
[55] F. Bournaud, B. G. Elmegreen, R. Teyssier, D. L. Block, and I. Puerari, ISM properties in hydrodynamic galaxy simulations: Turbulence cascades, cloud formation, role of gravity and feedback, Mon. Not. R. Astron. Soc. **409**, 1088 (2010).
[56] P. S. Marcus, S. Pei, C.-H. Jiang, J. A. Barranco, P. Hassanzadeh, and D. Lecoanet, Zombie vortex instability. I. A purely hydrodynamic instability to resurrect the dead zones of protoplanetary disks, Astrophys. J. **808**, 87 (2015).